Segmentation and Classification Using Logistic Regression in Remote Sensing Imagery

Hasnat Khurshid and Muhammad Faisal Khan

***Abstract*—This paper presents techniques for segmentation and change classification using logistic regression. The research was conducted on SPOT 5 multispectral multitemporal images covering the 2010 floods in Pakistan. Segmentation was performed to extract the built up area (BUA) from the satellite images and change detection was performed to find the damaged BUA. The damaged area was classified into three categories based on the extent of damage. The segmentation results were validated using statistical measures like precision, recall, and dice coefficient on available ground truth. The results of change classification were compared and found consistent with the manual assessment report produced by UNO experts using Worldview 1 satellite imagery with submeter resolution. The proposed scheme and results give an indication that SPOT 5 imagery can be used for fast automatic damage assessment and classification immediately after a natural calamity. The proposed change detection technique was also applied on Unites States Geographical Survey dataset. We compared our change detection results with established methods like change vector analysis, Principal component analysis using K-means and commercially available software Erdas Imagine on both the above-mentioned datasets. The comparison results suggest that our proposed algorithm performs better than the other methods.**

***Index Terms*—Change detection, logistic regression, satellite imagery, segmentation, SPOT 5.**

I. Introduction

NATURAL calamities such as floods, earthquake, hurricane, and tsunami have been consistently creating havoc in our planet and are unavoidable. Mankind has been trying to devise techniques to counter such calamities but has always been helpless against them. However, with the advent of modern technology, it is now possible to conduct an organized effort to mitigate the destruction and optimize the relief effort after any natural calamity. Pakistan has been struck twice by such disasters in the past decade in the form of 2005 earthquake and 2010 floods. Paucity of resources dictates the prioritization of relief work in accordance to the degree of damage in affected areas. During floods of August 2010, Pakistan with the help of local and foreign organizations such as SUPARCO [1] and UN-SPIDER [2] was able to use satellite images for damage assessment and categorization. This paper will utilize the existing techniques of mathematics and image processing to develop an automatic method for damage assessment using SPOT 5 multispectral multitemporal satellite images and compare the results with the assessment of experts. Use of remote sensing (RS) for damage assessment is not a new concept. The International Charter Space and Major Disasters [3] recognizes the effectiveness of satellite imagery to evaluate the damage caused by disasters [4]. Due to diversity of ground details in satellite images, there is no single generalized method for automatic damage assessment. A comparison of damage assessment techniques using RS data is presented by Tian and Zhang [5]. Damage assessment using RS imagery can be classified into number of categories depending upon the type of image/sensor, the platform on which the sensor was mounted, image availability and the type of technique used to assess the damage. In this paper, we shall discuss the techniques of damage assessment using high-resolution multitemporal multispectral satellite images.

The most basic and probably the most accurate form of damage assessment so far is through visual inspection [4]. For instance, the damage maps published by UNOSAT [6] after the 2006 Central Java earthquake were prepared from visual interpretation [7]. The visual inspection and comparison of satellite images are conducted by an experienced individual preferably familiar with the specific geographical area [8–10]. The visual inspection method though accurate is an extremely time consuming and difficult process. So, in order to be able to detect damage in short time and with reasonable accuracy automatic techniques of damage assessment are under rapid development.

Cognitive techniques use semantic features to identify an objects absence, presence, or change in the damaged areas [11]. Andre *et al.* use very high-resolution optical imagery to detect damages by investigating the changes in convex hulls of buildings before and after the Gujrat (India) earthquake of 2001 [12]. Tanathong *et al.* assuming a rectangular shape for all buildings used a combination of edge detection and region growing for extraction and damage assessment of buildings [13].

Pixel- or region-based change detection is also used frequently in damage assessment. Pixel-based damage assessment techniques either make use of a single pixel or a defined size neighborhood around the pixel for comparison of intensity level, variance, correlation, or mutual information. Change vector analysis (CVA) [14] is one of the established techniques used for change detection which uses the distance between the spectral values of two temporal pixels to quantify the change [15], [16]. Dou *et al.* use a certain sized neighborhood instead of single pixel for comparing two images [17]. Mutual Information is used by Gueguen *et al* to detect changes in SPOT 5 panchromatic images and thus analyse the urbanization in an area [18]. Jing-Fa *et al.* demonstrated change detection using

Manuscript received October 14, 2013; revised September 26, 2014; accepted September 30, 2014. Date of publication December 03, 2014; date of current version February 04, 2015.

The authors are with the National University of Sciences and Technology (NUST), Islamabad, Pakistan (e-mail: hasnat.PhD@mcs.edu.pk; mfaisalkhan@mcs.edu.pk).

Color versions of one or more of the figures in this paper are available online at http://ieeexplore.ieee.org.

Digital Object Identifier 10.1109/JSTARS.2014.2362769

TABLE I
DATASET CHARACTERISTICS

Sensor	SPOT 5
Resolution	2.5 m
Area	3600 km^2
Acquisition dates	Image 1 — Preflood 2009; Image 2 — Postflood 2010
Geographical area	Khyber Pakhtun Khua (KPK), Pakistan
Event covered	2010 floods

gray scale difference and gray scale variance difference of the corresponding neighborhood in two images covering Taiwan earthquake [19]. Similarly, seismic disaster was assessed by using the coherence, the difference of mean variance, and the difference of mean gray scale by Gueguen *et al.* [18]. Instead of working on spatial and spectral features, Bright and Vijayaraj used structural and textural features and tested it on hurricane Katrina data on IKONOS images [20]. Celik uses principal component analysis (PCA) with k-means for change detection in his work [21]. Survey papers are also available which present a brief survey of pixel-based change detection techniques and their comparison [22], [23].

The event covered by the research are the 2010 floods of Pakistan which have been recorded as one of the worst natural disasters in history. A sudden deluge of rain caused flash floods in Pakistan severely devastating the north western region of Pakistan. The flood covered the entire country and as per the official report of Pakistan's National Disaster Management Authority (NDMA) [24], the flood claimed almost 1400 lives and about 3.8 million people were affected across the country who had been deprived of their houses and belongings. Damage to infra structure was huge, as most of the houses had completely swept away in water. Most of the schools, hospitals, and other buildings and complexes had been severely damaged or completely destroyed. As per the initial assessment of Provincial Disaster Management Authority (PDMA) of Government of KPK approximately 545 739 households were affected by the rains and floods. 180 000 houses were completely destroyed, whereas 40 000 were damaged. In agriculture sector, crops destroyed exceeded 466 626 acres, whereas more than 10 000 livestock was destroyed. In communication infrastructure, about 2000 km of roads (major and link), 40 main bridges, 40 small bridges, and 90 foot bridges were destroyed. In buildings about 700 educational and 150 health facilities besides 158 government buildings were damaged due to flood. The proposed algorithm will assess and classify the damage and compare results with the ground truth.

II. MATERIALS

Two types of datasets are used in the study. The primary dataset constitutes two images taken before and after the flood. Each of the pre- and post-flood image covers an area of 60 km $\times$ 60 km (3600 km^2) with 2.5-m resolution. The main characteristics of the dataset are given in Table I and a subset of 83 km^2 of the image pair is shown in Fig. 1.

The second dataset was from United States Geographical Survey (USGS) Department [25] which comprises the temporal images of Landsat acquired in 1986 and 1992 covering Lake Tahoe, Nevada.

(a) (b)

Fig. 1. (a) Pre- and (b) post-flood, SPOT 5 satellite images of Pakistan covering the general area of Khyber Pakhtun Khua. The images are displayed using the natural color combination of four spectral bands of SPOT 5.

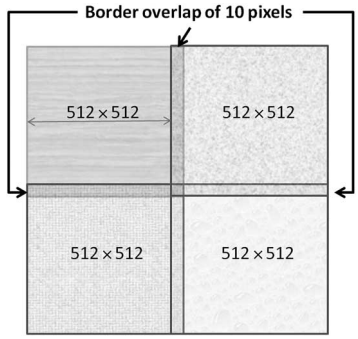

Fig. 2. Overlap of 10 pixels on each border for subimages of size 512 $\times$ 512.

III. METHODS

Damage assessment using multitemporal multispectral SPOT 5 images was conducted using image registration, segmentation, and change detection. The block diagram for the complete algorithm is shown in Fig. 3. The process of damage assessment starts with the initial preprocessing and registration of data after which the built-up area (BUA) is segmented from the image pair for damage assessment using proposed segmentation algorithm. Finally, the damage assessment is conducted and damage classification results are computed by categorization of damage density in geographical area.

A. Preprocessing and Registration

The temporal pre- and post-flood SPOT 5 multispectral image pair was available in four spectral bands. The pre- and post-flood images were spatially registered with manually selected control points using Erdas Imagine. Each registered spectral band image was then subdivided into 512 $\times$ 512 subimages for effective processing. Each subimage was given 10 pixels overlap on all of its borders as shown in Fig. 2.

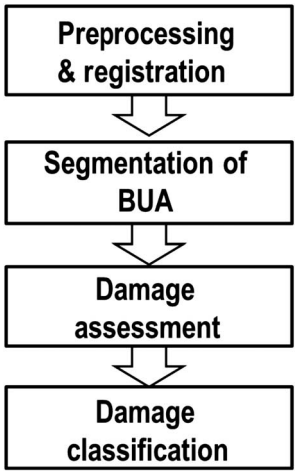

Fig. 3. Proposed algorithm for damage assessment.

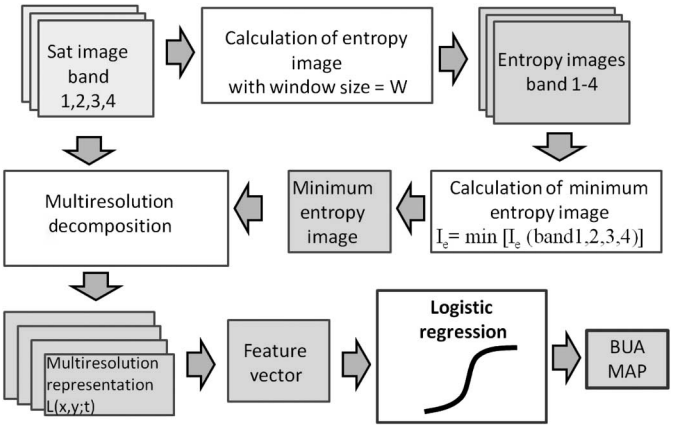

Fig. 4. Proposed algorithm for segmentation of BUA using high-resolution SPOT 5 multispectral satellite images.

Given the fact, that temporal images acquired at different dates are affected by different environmental conditions causing variation in intensity. To mitigate the effect of intensity variation, the images were intensity transformed using Power Law transformation. Power Law transformation function is given by the following equation:

$$I^t(i,j) = C \times I(i,j)^\gamma \tag{1}$$

where I and I^t are the original and transformed image, respectively. The value of γ was determined individually for each spectral band using corresponding control points and (1).

B. Segmentation of BUA

The widespread damage affected buildings, roads, and all sorts of vegetation. To restrict the damage assessment to infrastructure alone, there was a need to segment the BUA prior to damage assessment. For this purpose, logistic regression was used on spectral and information theoretic features combined with multiresolution decomposition to extract the BUA from the SPOT 5 satellite image. The proposed algorithm for segmentation of BUA using high-resolution SPOT 5 multispectral satellite images is shown in Fig. 4 and explained as follows.

1) Calculation of Entropy Image: As the first step, spectral images are converted to entropy images. Entropy of a pixel can be calculated by using the intensity values of its neighboring pixels within a defined window. So a pixel which has higher intensity variation in its neighborhood shall have higher entropy value and vice versa. This property of the pixel's neighborhood entropy can be used to segment geographical features which have peculiar *entropy signatures*. Entropy images were calculated using the following equation:

$$I_{eb} = -\sum_{i,j \in W} P(I_b(i,j))\log(P(I_b(i,j)) \tag{2}$$

where I_b is the intensity image in the spectral band $b\,(b = 1,2,3,4)$ and I_{eb} is the corresponding entropy image. W is the size of the sliding window.

The selection of window size is of critical importance for determining entropy signatures. A larger window size would unnecessarily increase the pixel entropy due to the inclusion of extra pixels around it, whereas a small window size can decrease the pixel entropy. The selection of W is hence dependent on the resolution of the satellite image and the spatial features of the local BUA. After careful analysis of the target area, size of roofs in BUA and the terrain, sliding entropy window size was selected to be $W = 5$ pixels.

2) Calculation of Minimum Entropy Image: In multispectral satellite images, each spectral band has different spectral signature for the same target objects. The spectral signatures are defined by the sensor's wavelength and the object's reflectance. Therefore, the entropy images I_{eb} will also be different when calculated for images in different spectral bands of the same geographic scene. It was observed that BUAs show higher entropy than other geographical features such as vegetation, ridges, and barren land. This higher entropy signature can be used for the segmentation of the BUA. Another important observation is that the higher entropy of BUA is consistent in the entropy images of all spectral bands in contrast to other geographical features which have varying entropy values in different spectral bands. This consistency of entropy signature of BUA can be used to increase the difference in the entropy of BUA and other geographical features. A minimum entropy image was obtained by selecting the minimum entropy value from the entropy images of all spectral bands using following equation:

$$I_e(i,j) = \min[I_{e1}(i,j), I_{e2}(i,j), I_{e3}(i,j), I_{e4}(i,j)] \tag{3}$$

where I_e is the minimum entropy image and I_{e1-4} are the four entropy images corresponding to each of the four spectral bands.

This minimum entropy image now has a significant difference in the entropy values of BUAs and other geographic features. Furthermore, this step also effectively segregates the BUA from geographical features (such as "small fields") which had similar geometric appearance as houses in BUAs.

3) Multiresolution Decomposition: In step 3 of the proposed algorithm, multiresolution versions $L(t)$ of the minimum entropy image I_e at different scales t were computed using wavelet transform. Wavelet transform effectively achieves

space frequency localization and can be used for multiresolution decomposition of image. Wavelet transform is performed by convolving the original image with a family of basis function and is given as follows:

$$L(t) = \frac{1}{\sqrt{MN}} \sum_{i=0}^{M-1} \sum_{j=0}^{N-1} I_e(i,j)\psi_{m,n;t}(i,j) \tag{4}$$

where $L(t)$ are the multiresolution versions of minimum entropy image I_e at different scale levels t. $\psi_{m,n;t}(i,j)$ is the family of basis functions used for wavelet decomposition and $M \times N$ is the size of the image I_e.

4) Feature Vector and Logistic Regression: The feature vector was made with the combination of the intensity values in four spectral bands and the entropy value decomposed till three scale levels thus giving a total of 15 features. The decomposition scale plays an important role in classification. A higher scale value (causing more decomposition) will tend to under classify the isolated huts and scattered houses, which is good when segmentation of only major towns and cities is required. On the other hand, a lower scale value will result in more false positives. Binomial logistic regression was used for classification of pixels into BUA and non-BUA pixels. The probability P for a pixel to be classified as BUA pixel, using logistic regression is given as

$$P(X_{(i,j),k} \in BUA) = \frac{1}{1 + e^{-\left(a + \sum_{k=1}^{K} b_k X_{(i,j),k}\right)}} \tag{5}$$

where $X_{(i,j),k}$ is the feature vector corresponding to a pixel of index (i,j) and K is the total number of features. Model parameters a and b are calculated using maximum likelihood. The classified pixels were then used to produce a BUA map.

C. Damage Assessment

The proposed damage assessment and classification method are based on the combination of various pixel-based change detection techniques. Six change detection techniques were used in each spectral band thus giving a total of 24 features. The change detection techniques used are explained in the following paragraphs. Symbols I_{pre} and I_{post} will be used for denoting the pre- and post-flood images, respectively.

1) Absolute Image Difference: The absolute image difference (AID) is calculated by subtracting the intensity values of corresponding individual pixels in pre- and post-calamity images in each spectral band. It is given as

$$I_{AID}(i,j) = |I_{pre}(i,j) - I_{post}(i,j)|. \tag{6}$$

2) Mean Square Distance (MSD): In natural calamities, the damage is always caused to an area which is much larger than that of a single pixel (2.5 m^2 in our case); therefore, it is important that the change is detected in the near neighborhood of a pixel. To incorporate the neighborhood, mean square distance (MSD) was used to calculate the difference in the images considering a neighborhood window of size W. The size and shape of the neighborhood are of critical importance and have to be set according to image resolution and size of ground objects. MSD is given by following formula:

$$I_{MSD} = \frac{\sum_{i,j \in W} \left(I_{pre}(i,j) - I_{post}(i,j)\right)^2}{W - 1} \tag{7}$$

where I_{MSD} is the image with MSD.

3) Pearson's Correlation Coefficient: Pearson's correlation coefficient (PCC) also incorporates the neighborhood of the pixel around it with a given window size W. PCC is independent of linear scaling in intensity and hence provides a better similarity measure for comparing images which are acquired under different lighting conditions. It is given as

$$I_{PCC} = \frac{\sum_W \left[\left(I_{(pre,W)} - \bar{I}_{(pre,W)}\right)\right.}{\sqrt{\sum_W \left(I_{(pre,W)} - \bar{I}_{(pre,W)}\right)^2}} \times \frac{\left.\left(I_{(post,W)} - \bar{I}_{(post,W)}\right)\right]}{\sqrt{\sum_W (I_{(post,W)} - \bar{I}_{(post,W)})^2}} \tag{8}$$

where W represents the sliding window. $\bar{I}_{pre,W}$ and $\bar{I}_{post,W}$ are sample means of images $\bar{I}_{pre,W}$ and $\bar{I}_{post,W}$ within the window W. The range of *PCC* is between -1 and $+1$, where -1 indicates negative relation and $+1$ indicates positive relation. The PCC was calculated for I_{pre} and I_{post} over a sliding window of size $W = 5$.

4) Entropy Difference: The entropy of pixel neighborhood in a window size of W was also used as a feature for change detection. The formula for calculating the entropy image *EI*, using a sliding window operation is given as

$$EI = -\sum_{i,j \in W} p(I(i,j)) \log p(I(i,j)) \tag{9}$$

where p is the probability function. The image of entropy difference (ED) I_{ED} of two entropy images EI_{pre} and EI_{post} can be computed as

$$I_{ED} = |EI_{pre} - EI_{post}| \tag{10}$$

5) Normalized Mutual Information: Normalized mutual information (NMI) measures the similarity or difference based on the amount of mutual information content of the images. It is given by following equation:

$$I_{NMI} = \frac{H(I_{pre}(i,j)) + H(I_{post}(i,j))}{H\left(I_{pre}(i,j), I_{post}(i,j)\right)} \tag{11}$$

where $i,j \in W$. H is the entropy function and $H(I_{pre}(i,j) \cdot I_{post}(i,j))$ represents the joint entropy over a sliding window W. The range of NMI is between [0, 1], where the value of $NMI = 0$ depicts dissimilarity, and the value of $NMI = 1$ indicates that both the images are exactly the same. NMI was calculated for the corresponding image pair in each spectral band using (11). The major drawback of using this feature is that it is computationally expensive and slows down the overall damage assessment algorithm.

6) PCA: PCA is a statistical technique for finding the relation in multidimensional data. In order to apply the PCA for damage assessment, we used the intensity values of the pre- and post-flood images (I_{pre} and I_{post}) as the input data. The pre- and post-flood images were first converted into column vectors $\vec{I}_{pre}$ and $\vec{I}_{post}$ and then 2×2 covariance matrix was calculated using the following formula:

$$\text{Cov Matrix} = \begin{bmatrix} COV(\vec{I}_{pre}, \vec{I}_{post}) & COV(\vec{I}_{pre}, \vec{I}_{pre}) \\ COV(\vec{I}_{post}, \vec{I}_{post}) & COV(\vec{I}_{post}, \vec{I}_{pre}) \end{bmatrix} \quad (12)$$

where $COV(\vec{I}_{pre}, \vec{I}_{post})$ is the covariance between vectors $\vec{I}_{pre}$ and $\vec{I}_{post}$.

After obtaining the covariance matrix, the eigenvectors and eigenvalues of the covariance matrix are calculated. The eigenvectors and eigenvalues are denoted as follows:

$$eigenvectors: \; E_1 = \begin{bmatrix} E_{11} \\ E_{12} \end{bmatrix} \quad \text{and} \quad E_2 = \begin{bmatrix} E_{21} \\ E_{22} \end{bmatrix} \quad (13)$$

$$eigenvalues: \; EV = \begin{bmatrix} EV_{11} \\ EV_{12} \end{bmatrix}. \quad (14)$$

The eigenvector with highest eigenvalue corresponds to the principal component one (PC1), which depicts the highest relationship among the given data. Feature vector for PCA (FV_{PCA}) was formed using the eigenvectors sorted as per eigenvalues

$$FV_{PCA} = \begin{bmatrix} E_{11} & E_{21} \\ E_{12} & E_{22} \end{bmatrix}. \quad (15)$$

Following equation was used to obtain the transformed vectors $\vec{I}_{PC1}$ and $\vec{I}_{PC2}$

$$[\vec{I}_{PC1}\vec{I}_{PC2}]^T = FV_{PCA}^T \times [\vec{I}_{pre}\vec{I}_{post}]^T \quad (16)$$

where T represents the transpose operation. The transformed data are now on different coordinates depending on the relationship between the two dimensions of the data. For similar images, PC1 depicts the highest relation between the two images and can be used as a measure for similarity whereas PC2 which is orthogonal to PC1 can be used for the measure of dissimilarity. The transformed vector $\vec{I}_{PC2}$ was reshaped to image dimensions to obtain the dissimilarity depicting image I_{PC2}.

7) Damage Classification using Multinomial Logistic Regression: The final feature vector $D(i,j)$ for change detection was made by combination of all 6 similarity measures in each of the four spectral band thus giving a total of 24 features per pixel. The feature vector was used with multinomial logistic regression (MLR) to classify the damaged area into three classes of damage as *high*, *moderate*, and *low*. For each class, training data were provided from 24 selected towns in the image to calculate the regression coefficients. The selected towns are marked in Fig. 10. The overall damage class of a particular town/village was determined by taking the mode of the damaged pixels' classes within that town/village. MLR is performed by keeping one category as reference and regressing all other categories using this reference. The probability that a pixel (i,j) belongs to a particular damage category c is given as

$$P\left(Z_{(i,j)} \in c\right) = \frac{e^{-\left(a_c + \sum_{k=1}^{K} b_{ck} Z_{(i,j),k}\right)}}{1 + \sum_{c=2}^{C} e^{-\left(a_c + \sum_{k=1}^{K} b_{ck} Z_{(i,j),k}\right)}} \quad (17)$$

where $Z_{(i,j),k}$ is the feature vector, (i,j) is the pixel index, K is the total number of features, and C is the total number of categories.

For the first category, $c = 1$, the equation is given as

$$P(Z_{(i,j)} \in c = 1) = \frac{1}{1 + \sum_{c=2}^{M} e^{-\left(a_c + \sum_{k=1}^{K} b_{ck} Z_{(i,j),k}\right)}}. \quad (18)$$

Pseudocolors were used to present the the damage mask displaying the three classes of damage in selected geographical area.

D. Validation

Validation was conducted for proposed segmentation as well as damage categorization scheme. The segmentation results of proposed algorithm were compared with manually segmented BUA mask. Considering the manual segmentation as ground truth, the total number of false positive, true positive, and false negative pixels were computed for proposed segmentation. Using these pixels count, Precision and Recall were calculated using the following equations:

$$\text{Precision} = \frac{TP}{TP + FP} \quad (19)$$

$$\text{Recall} = \frac{TP}{TP + FN} \quad (20)$$

where *TP* is true positive, *FP* is false positive, and *FN* is false negative pixel count. The dice coefficient [5] was also computed between automatic and manually segmented BUA. In addition to manual segmentation, the results produced were also compared with the supervised classification of Erdas Imagine and MLR on spectral features using the above-mentioned performance measures. Supervised classification was performed using Erdas Imagine with the help of same training samples as used in the proposed algorithm. The damage classification map was compared with the damage overview report of UNOSAT as shown in Fig. 5. The damage review report of UNOSAT was based on expert visual interpretation of damage using Worldview 1 satellite imagery with submeter resolution. The image was taken immediately after the floods on August 2, 2010, which allowed the interpreters to effectively estimate the damage without loss of information. The report categorizes the damage based on the degree of damage to buildings in selected affected towns. The UNOSAT report covers 16 towns evaluated in proposed damage assessment algorithm and hence can serve as a suitable benchmark for damage categorization of proposed algorithm in given towns. Change detection and damage

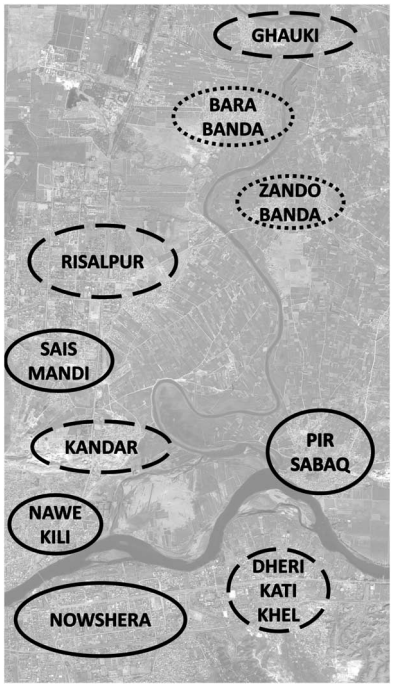

Fig. 5. Extracts from 2010 flood damage overview report of Khyber Pakhtun Khua (KPK), Pakistan produced by UNOSAT. The damage to towns have been categorized as high (solid border), moderate (dashed border), and low (dotted border) being shown in red, green, and blue color, respectively.

categorization results of proposed scheme were compared with existing techniques of CVA and Celik's [21] PCA K-means technique.

IV. Results and Discussion

A. BUA Segmentation

The effectiveness of proposed algorithm was tested for segmenting the BUA area in the SPOT 5 multispectral satellite image. The segmentation results of a selected image patch of 17 km^2 are presented in the paper. The selected image patch constitutes 10 subimages of 512×512 (around 1.7 km^2) size. One subimage of each band is shown in top row of Fig. 6. The result of entropy images obtained from each band of one subimage is shown in the bottom row of Fig. 6. It can be seen from the entropy images that the BUA displays higher entropy in all spectral bands, whereas other geographic features such as fields and barren land have lower entropy. Furthermore, the prominent water body, i.e., the river has the least entropy in the image especially in spectral bands 1 and 4. The minimum entropy image obtained using (3) of step 2 is shown in Fig. 7. The difference in the pixel entropy of BUA and other geographic features has significantly increased in minimum entropy image. The multiresolution decomposition of minimum entropy image using (4) of step 3 can be seen in Fig. 7. Finally, the segmentation masks for BUA using proposed algorithm and ground truth are shown in Fig. 8. It can be seen from the segmentation masks that the proposed algorithm produces an effective mask of BUA with reasonable accuracy.

The quantitative validation results and comparisons are given in Tables II and III, and Fig. 9. The final values of precision, recall, and dice coefficient over the entire image patch using proposed algorithm are a reasonable segmentation result for a satellite image with 2.5-m resolution. The result was compared with two other approaches which used spectral classification. In the first approach, MLR was used and in the second approach Erdas Imagine was used for classification only with the spectral features. In both cases, a lot of false positives were generated resulting in a low *Recall* result. Performance measures as shown in Table III support the superior performance of proposed algorithm in comparison to other supervised classification approaches.

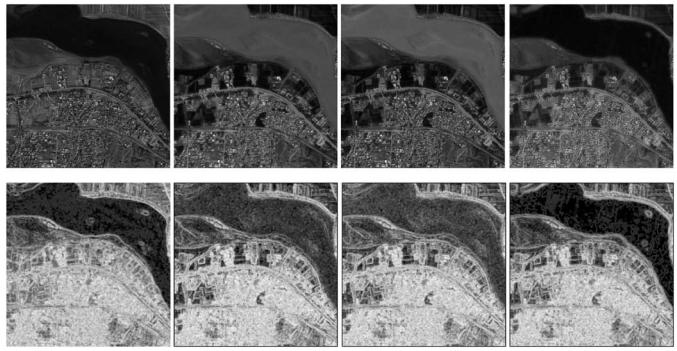

Fig. 6. Multispectral subset image (1.7 km^2) in four spectral bands (bands 1–4 from left to right of top row) and there corresponding entropy images (bottom row) taken with a penta-pixel sliding window. Note that BUA has higher entropy than other geographical features (such as fields and river) in all spectral bands.

(a)

(b)

Fig. 7. (a) Minimum entropy image of the 17 km^2 SPOT 5 image patch obtained by combining entropy images of all spectral bands using (3). (b) DWT decomposition of minimum entropy image using (4).

B. Damage Analysis

The 24 towns selected for the damage assessment are marked in Fig. 10 and the damage categorization of these 24 towns is shown in Fig. 10. When comparing the categorization of proposed algorithm with that of UNOSAT report in Fig. 5, it

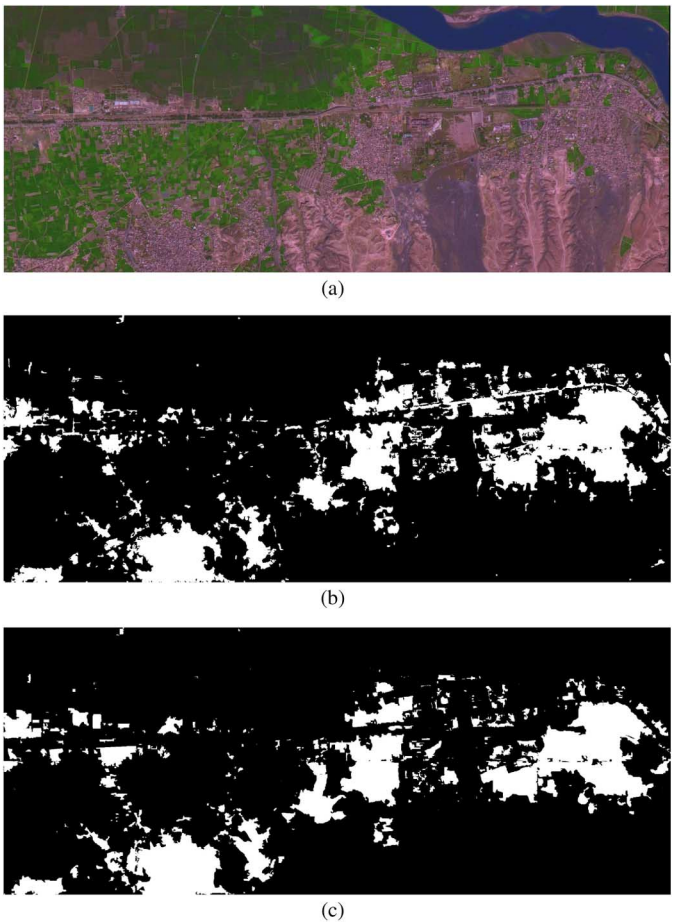

Fig. 8. (a) Original SPOT 5 image patch of 17 km^2 area. (b) Segmented BUA mask using wavelet decomposition. (c) Segmented BUA mask using manual segmentation.

TABLE II
VALIDATION RESULTS OF BUA SEGMENTATION WITH 1.7 KM^2 SUBIMAGES

Subimage	Recall	Precision	DICE
1	0.81131	0.73625	0.77196
2	0.54461	0.54343	0.54402
3	0.88947	0.87544	0.88239
4	0.91733	0.40318	0.56016
5	0.9748	0.83368	0.89873
6	0.74324	0.89307	0.8113
7	0.87667	0.94343	0.90883
8	0.80156	0.92223	0.85767
9	0.86476	0.83674	0.85052
10	0.82721	0.9469	0.88302

can be seen that the proposed damage classification map is similar to the damage map produced by UNOSAT. The towns and residential areas closer to the main river *Kabul* such as *NaweKili*, *Nowshera*, and *PirSabaq* are more severely damaged in comparison to the areas away from the river. The town of *Ghauki-east*, however, has been identified as less damaged in the results of proposed algorithm whereas the same has been reported as moderately damaged by UNOSAT. This difference

TABLE III
COMPARISON OF RESULTS BETWEEN SPECTRAL MLR, ERDAS IMAGINE, AND PROPOSED ALGORITHM

Algorithm	Recall	Precision	DICE
Spectral MLR	0.69922	0.68232	0.57012
Erdas imagine	0.73291	0.75682	0.63070
Proposed algo	0.86065	0.82024	0.83996

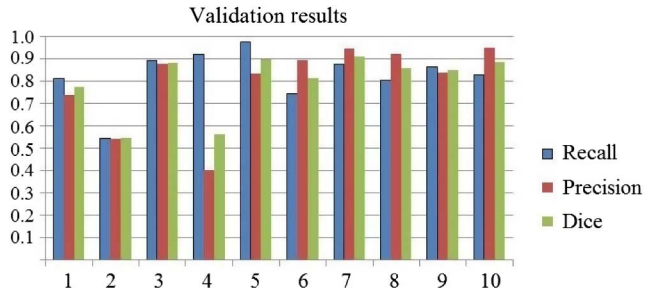

Fig. 9. Comparison of validation results of individual subimages of 1.7 km^2 area using proposed algorithm.

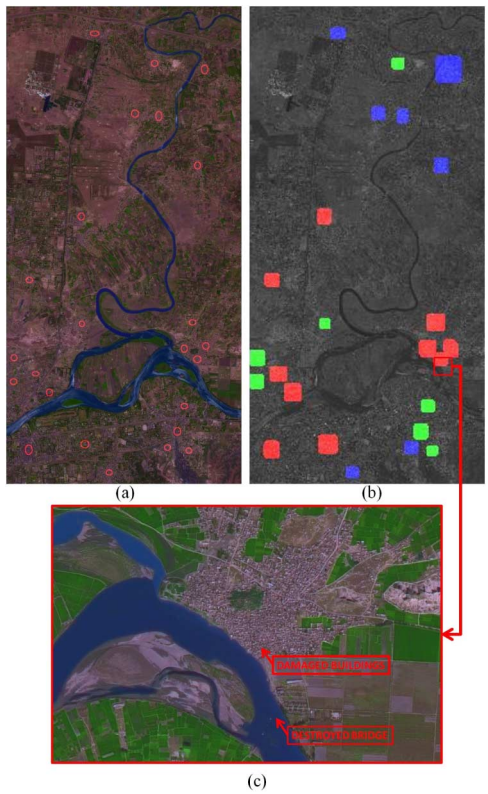

Fig. 10. (a) Selected areas for damage assessment. A total of 24 towns encircled in red color were selected for damage assessment and categorization. (b) Damage categorization of selected towns in flood affected areas using proposed algorithm. The colors red, green, and blue depict high, moderate and low damage, respectively. The sizes of sample area for each town have been adjusted in proportion to the amount of constructed area to ensure a fair categorization of damage. (c) Damaged area of Pir Sabaq at higher zoom level. The destroyed bridge and damaged buildings can be seen in the area as it had the highest damage in the 2010 floods.

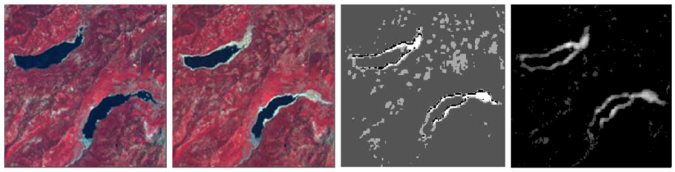

Fig. 11. Comparison of change detection in dataset of USGS [25]. (a) Before image. (b) After image. (c) Celik's PCA K-means algorithm ($k = 4$). (d) Proposed algorithm.

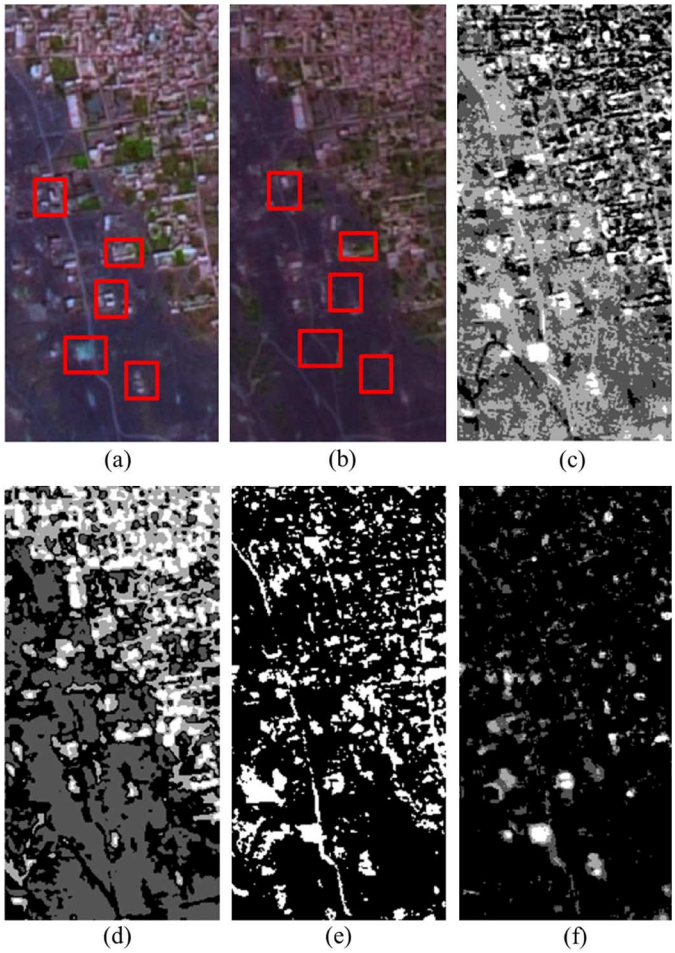

Fig. 12. Comparison of change detection in a subset of own dataset. Few ground truth changes have been marked with red boxes which can be easily detected visually. (a) Before image. (b) After image. (c) CVA. (d) Celik's PCA K-means algorithm ($k = 4$). (e) Erdas Imagine's change detection with 30% change threshold. (f) Proposed algorithm.

in results is due to the fact that the proposed algorithm was performed on the satellite imagery taken few months after the flood, whereas UNOSAT's report was based on satellite imagery immediately taken after flood. Furthermore, the resolution of SPOT 5 imagery is not sufficient for precise damage assessment and can only give a broad estimate of damage. Considering UNOSAT's report as ground truth, 15 out of 16 towns have been correctly categorized in damage which is a very encouraging result for automatic damage assessment performed on 2.5-m satellite image.

TABLE IV
COMPARISON OF DAMAGE CATEGORIZATION RESULTS

Town	Damage categorization			
	UNOSAT	CVA	Celik's PCA	Proposed Algorithm
Ghauki-east	Moderate	Low	Moderate	Low
Ghauki-west	Moderate	Low	High	Moderate
Bara Banda-east	Low	High	High	Low
Bara Banda-west	Low	Low	High	Low
Risalpur	Moderate	Moderate	High	Moderate
Kandar	Moderate	Low	High	Moderate
Nawe Kili-east	High	Low	Moderate	High
Nawe Kili-west	High	Low	High	High
Nowshera-east	High	High	Moderate	High
Nowshera-west	High	Moderate	Moderate	High
Pir Sabaq-north	High	Low	Moderate	High
Pir Sabaq-east	High	Moderate	High	High
Pir Sabaq-west	High	Moderate	High	High
Pir Sabaq-south	High	High	Low	High
Dheri Kati-north	Moderate	Low	High	Moderate
Dheri Kati-sorth	Moderate	Low	High	Moderate

The proposed scheme was also compared with the existing change detection techniques of CVA, commercial software Erdas imagine and Celik's [21] PCA-based work. All schemes were set to detect changes which were then classified into four classes. The change detection results on USGS dataset [25] as well as a subset image of own dataset are shown in Figs. 11 and 12, respectively. It can be seen that the proposed scheme generates lesser false positives. The combination of spatial and spectral change detection features enables the proposed scheme to correctly classify the change.

The damage categorization of selected flooded villages computed using the change detection techniques of Celik, CVA, and the proposed algorithm are listed in Table IV along with UNOSAT's report. It can be seen that the damage categorization results of proposed algorithm are very close to the UNOSAT's report in comparison to other techniques.

V. CONCLUSION

Segmentation and classification of multitemporal multispectral SPOT 5 satellite images was presented using logistic regression. The registration process was conducted using commercial software and corresponding control points. Segmentation of BUA were performed using entropy and spectral values at lower scale versions using DWT. Finally, the damage assessment and categorization was conducted within the BUA using MLR on a combination of difference measures techniques. The results of proposed algorithm were evaluated using visual interpretation, statistical flood damage data produced by government agencies, and the damage reports of UNOSAT. Comparison of results was made with commercial and existing techniques of segmentation and damage assessment. The damage results produced were found consistent with ground facts and hence give a lead for using SPOT 5 images for damage assessment.

ACKNOWLEDGMENT

The authors would like to thank Space and Upper Atmospheric Commission (SUPARCO) Pakistan and USGS for provision of data and image analysis.

REFERENCES

[1] Space and upper atmosphere research commission of Pakistan [Online]. Available: http://www.suparco.gov.pk/, accessed on Sep. 2013.
[2] United Nations Space Based Information for Disaster Management and Emergency Response (UN-SPIDER) [Online]. Available: http://www.un-spider.org/, accessed on Sep. 2013.
[3] The International Charter' Space and major Disasters' [Online]. Available: http://www.disasterscharter.org/, accessed on Sep. 2013.
[4] S. Battiston *et al.*, "Rapid EO disaster mapping service: Added value, feedback and perspectives after 4 years of charter actions," in *IEEE Proc. Int. Geosci. Remote Sens. Symp.*, 2005, vol. 6, pp. 4373–4378.
[5] Y. F. Tian and J. F. Zhang, "Techniques for seismic damages assessment by using remotely sensed images," in *Proc. Int. Geosci. Remote Sens. Symp. (IGARSS)*, 2004, vol. 2, pp. 1422–1425.
[6] Unitars Operational Satellite Applications Programme (UNOSAT) [Online]. Available: http://www.unitar.org/unosat/, accessed on Sep. 2013.
[7] M. Matsuoka, H. Miura, and F. Yamazaki, "Identification of damaged areas due to the 2006 central java, Indonesia earthquake using satellite optical images," in *Proc. Urban Remote Sens. Joint Event*, 2007, pp. 1–5.
[8] P. Gamba and F. Casciati, "GIS and image understanding for near-real-time earthquake damage assessment," *Photogramm. Eng. Remote Sens.*, vol. 64, pp. 987–994, 1998.
[9] M. Matsuoka and F. Yamazaki, "Visual damage interpretation of buildingsin Bam city using quickbird images following the 2003 Bam, Iran, earthquake," in *Proc. Earthquake Spectra*, 2005, vol. 21, pp. S329–S336.
[10] T. A. de C. Foley and R. S. Keiko Saito, "Visual damage assessment using high-resolution satellite images following the 2003 Bam, Iran, earthquake," in *Proc. Earthquake Spectra*, 2005, vol. 21, pp. S309–S318.
[11] T. Wang and C. Zhang, "Cognitive model based method for earthquake damage assessment from high-resolution satellite images: A study following the Wenchuan earthquake," in *Proc. 6th Int. Conf. Nat. Comput.*, 2010, pp. 2079–2083.
[12] G. Andre, L. Chiroiu, C. Mering, and F. Chopin, "Building destruction and damage assessment after earthquake using high resolution optical sensors the case of the Gujarat earthquake of January 26, 2001," in *Proc. IEEE Int. Geosci. Remote Sens. Symp. (IGARSS)*, 2003, vol. 4, pp. 2398–2400.
[13] K. T. Rudahl, S. Tanathong, and S. E. Goldin, "Object oriented change detection of buildings after the Indian ocean tsunami disaster," in *Proc. 5th Int. Conf. Electric. Eng. Electron. Comput. Telecommun. Inf. Technol.*, 2008, vol. 1, pp. 65–68.
[14] W. Malila, "Change vector analysis: An approach for detecting forest changes with Landsat," in *Proc. 6th Annu. Symp. Mach. Process. Remotely Sensed Data*, Purdue University, West Lafayette, IN, USA, Jun. 1980, pp. 326–335.
[15] O. A. C. Jnior, R. F. Guimares, A. R. Gillespie, N. C. Silva, and R. A. T. Gomes, "A new approach to change vector analysis using distance and similarity measures," *Remote Sens.*, vol. 3, pp. 2473–2493, 2011.
[16] F. B. Balcik and C. Goksel, "Determination of magnitude and direction of land use/land cover changes in terkos water basin, Istanbul," in *Proc. Int. Archives Photogramm. Remote Sens. Spatial Inf. Sci.*, 2012, vol. 39.
[17] Y. F. Tian, A. X. Dou, and J. F. Zhang, "Retrieve seismic damages from remote sensing images by change detection algorithm," in *Proc. IEEE Int. Symp. Geosci. Remote Sens.*, 2003, vol. 2, pp. 2407–2409.
[18] D. Ehrlich, L. Linlin, L. Gueguen, and M. Pesaresi, "Urbanization analysis by mutual information based change detection between spot 5 panchromatic images," in *Proc. 6th Int. Workshop Anal. Multitemp. Remote Sens. Images*, 2011, pp. 157–160.
[19] T. Xia-xin, Z. Jing-Fa, and X. Li-li, "Change detection of earthquake-damaged buildings on remote sensing image and its application in seismic disaster assessment," in *Proc. IEEE Int. Symp. Geosci. Remote Sens.*, 2003, vol. 4, pp. 2436–2438.
[20] E. A. Bright and V. Vijayaraj, "Rapid damage assessment from high resolution imagery," in *Proc. IEEE Int. Symp. Geosci. Remote Sens.*, 2008, vol. 4, pp. III-499–III-502.
[21] T. Celik, "Unsupervised change detection in satellite images using principal component analysis and k-means clustering," *IEEE Geosci. Remote Sens. Lett.*, vol. 6, pp. 772–776, Oct. 2009.
[22] J. F. Zhang and Y. F. Tian, "Techniques for seismic damages assessment by using remotely sensed images," in *Proc. IEEE Int. Symp. Geosci. Remote Sens.*, 2004, vol. 2, pp. 1422–1425.
[23] M. Crawford, E. Rathje, and K. Woo, "Comparison of earthquake damage evaluation using change detection and thematic classification," in *Proc. 3rd Int. Workshop Remote Sens. Disaster Response*, Chiba, Japan, 2005.
[24] National Disaster Management Authority [Online]. Available: http://www.ndma.gov.pk/, accessed on Sep. 2013.
[25] Southwest U.S. change detection images from the eros data center [Online]. Available: http://geochange.er.usgs.gov/sw/changes/natural/reno-tahoe/, accessed on Sep. 2014.

Hasnat Khurshid received the B.S. and M.S. degrees in electrical engineering from the National University of Sciences and Technology (NUST), Islamabad, Pakistan, in 2002 and 2010, respectively.

Currently, he is working as a Ph.D. Scholar with NUST. His research interests include digital image processing, remote sensing, and machine learning.

Muhammad Faisal Khan received the B.S. degree in electrical engineering from the University of Engineering and Technology, Lahore, Pakistan, and the M.S. and Ph.D. degrees in electrical and computer engineering from Georgia Institute of Technology, Atlanta, GA, USA, in 1994, 2004, and 2008, respectively.

He is working as an Assistant Professor with the College of Signals, National University of Sciences and Technology (NUST), Islamabad, Pakistan.